Applying an Anomaly-Detection Algorithm for Short-Term Land Use and Land Cover Change Detection Using Time-Series SAR Images

Junping Qian[1]
Guangzhou Institute of Geography, Xianliezhong Road #100, Guangzhou, China, 510070 and School of Geography and Planning, SunYet-Sen University, Xingang West Road #135, Guangzhou, China, 510275

Xia Li
School of Geography and Planning, SunYet-Sen University, Xingang West RD. 135#, Guangzhou, China, 510275

Stephen Liao
Department of Information System, City University of Hong Kong, Tat Chee Avenue, Kowloon, Hong Kong, China

Anthony-Gar-on Yeh
Center of Urban Planning and Environment Management, The University of Hong Kong, Pok Fu Lam Road, Hong Kong, China

Abstract: In this study, short-term land use and land cover (LULC) changes caused by human activity were considered as spatial-temporal abnormalities in time-series images. A density-based anomaly detection (DBAD) algorithm was designed to detect the changes. Then the algorithm was applied to RADARSAT time-series images, and synchronous field surveying was performed for validation. The results showed that the DBAD algorithm was good at detecting in-progress construction and newly built-up parcels, with an error of less than 13.3%. A lower detection error was achieved for woodland areas, and a larger error for built-up areas and for some mixed-use land parcels due to the complexity of the parcels.

INTRODUCTION

The Pearl River Delta of southern China has undergone rapid urbanization since 1980. A rough estimation by Li (2003) revealed that there was a more than 20% change in land use and land cover (LULC) in this area each year. Most LULC changes were from cultivated land to construction areas. Other changes included those from bare land to built-up areas, cultivated land to fish ponds, etc. Although the Pearl River

[1]Corresponding author; email: qian@gdas.ac.cn; jpqian123@126.com

GIScience & Remote Sensing, 2010, **47**, No. 3, p. 379–397. DOI: 10.2747/1548-1603.47.3.379

Delta has experienced such rapid and drastic LULC changes, little research has been produced on short-term LULC changes, owing to the lack of appropriate measurement capacity. Located in the cloudy and rainy area of southern China, the Pearl River Delta is subject to year-round cloud cover and high humidity. This makes short-term LULC monitoring almost impossible with traditional optical remote sensing. However, synthetic-aperture radar (SAR) works in microwave bands and can penetrate the clouds and rain. This enables SAR to observe under all weather conditions and thus to complement optical remote sensing. Several satellites with SAR are available for periodic observations, including the ERS-1, 2 (C band, VV polarization); the JERS-1 (L band, HH polarization); and the ASAR (C band, multi-mode, multi-polarization) satellites. At the time of our research, the highest resolution SAR was the Canadian RADARSAT (fine-beam mode, pixel size 4.6 m, spatial resolution 6.2 m). All these SAR systems provide stable and continuous records of the Earth's surface even in cloudy and rainy areas. This meant that LULC monitoring could be carried out in almost real time. This is likely to be of great interest to LULC scholars and to urban scientists.

Although Nagler and Rott's (2000) and Stabel and Fischer's (2001) research attested to the success of repeat-pass SAR imagery in continuous land-surface monitoring under all weather conditions, several unresolved problems remained for all-weather monitoring of LULC using a time series of SAR images. Praks et al. (2001) pointed out that images acquired at different times are inevitably affected by changed observation conditions. For example, the air humidity, rainfall, cloud cover, or observation bias caused by the instability of the platform and sensors can exert influence on the observation results. In addition, Quegan et al. (2000) also suggested the possibility of physical and biological changes of the land surface during the observation period, such as tree growth and the blooming of vegetation that occur mostly in agricultural or vegetation-covered areas. To avoid these extra-essential changes or biases, researchers usually choose remote sensing images collected from the same platform and acquired using the same parameters. Some researchers even choose images taken in the same season and under the same weather conditions so that the imagines' differences owing to the observation system and environment can be minimized. In the case of short-term LULC monitoring, the time-series remote sensing images are inevitably acquired in different seasons and under different environmental conditions. Thus, for every two scenes of the images, both the LULC change and the extra-essential changes or biases caused by the environment and by the observation system are faithfully recorded in the images. To identify LULC changes in time-series images, all extra-essential changes or biases must be eliminated.

As in the cases of Song et al.'s (2001) and Chen et al.'s (2005) work, image variations caused by platform and environment are usually eliminated by radiation rectification. The variations caused by the physical or biological changes of the land surface are more difficult to remove, however. Moreover, the latter are sometimes visible in time-series images and can cause significant confusion in short-term LULC change detection. Qian et al. (2007) found that certain temporal patterns existed in multitemporal images and that these patterns could be utilized in LULC change detection. To achieve this, however, the images must be precisely radio-calibrated. In most cases, this is not an easy proposition.

Anomalies, also referred to as outliers, are defined by Hawkins (1980) and Barnett and Lewis (1994) as data that differ exceptionally from normal data. Anomaly detection

algorithms were accordingly designed to identify the small group of events that belong neither entirely to the background nor to any clustering of the dataset. Anomaly detection was originally introduced into remote sensing for hyperspectral analysis and for precise target identification. It has been found that distinct spectral signals could be located by anomaly detection algorithms even without any background knowledge or prior information (Chen et al., 2006; Lu et al., 2006). After this revelation, anomaly detection was adopted by geographers for the detection of geographic change. For example, Chen and Li (2006) applied outlier change detection algorithms to a filtered multi-scale digital elevation model and detected anomalous coastal terrain changes at different scales. Gauthier et al. (2001) used sliding-window differencing schemes and spatial pixel-profile analysis to examine the small-scale anomalies of linear objects in high-resolution images. Furthermore, Liu and Zhang (2006) assumed that the background textures of the images could be modeled by Gaussian distributions and that the anomaly distribution of manmade objects would be significantly different from that of the background.

As summarized by Kou et al. (2006), anomalies in remote sensing so far have been mostly considered as spatial objects with features significantly different from those of their neighborhoods. This means only objects having features distinct from those of their neighboring objects would be detected as anomalies. This is sometimes not the case in real situations. In agricultural land (a paddy field for example), there are usually several growing stages, including transplanting, sprouting, tasseling, and harvesting. In each stage, the height and the leaves of the plants change significantly, as does the water content in the field. Because of the change in the paddy fields and the distinguishable difference between the fields and their neighborhoods, paddy fields tend to be mistaken as anomaly-changed areas when generally defined anomaly algorithms are used. This can lead to considerable false or failed alarms in short-term LULC change detection.

In this study, the spatial and temporal anomalies of LULC change in time-series images were analyzed. Then the short-term LULC change was defined as an anomaly at the global scale. A density-based anomaly detection (DBAD) method was then proposed for short-term LULC change detection, and the detection results were verified.

METHODOLOGY

Change and Anomalies

The backscattering variation in time series of SAR images may have several causes, including the instability of the observing platform or sensors, environmental changes, the seasonal variation of vegetation, and LULC change caused by human activity. To identify the "real" LULC changes from the changes in the time-series images, we must identify distinctive features to allow for discrimination. Table 1 lists the main possible factors that can cause changes in time-series images and their characteristics.

As Table 1 shows, changes caused by the observation system are usually systemic and gradual and lead to consistent variation on the whole scene of the image. Therefore, changes of the observation system caused only temporal anomalies in the time-series images. As for changes in the atmospheric environment and land surface,

Table 1. Factors That Cause Changes in Time-Series Images and Their Characteristics

	Factors	Change type	Characteristics	Anomaly	
				Temporal anomaly	Spatial anomaly
1	Instability of observation system	Systemic change	Slow and gradual change, caused consistent backscattering deviation on entire scene of images	√	×
2	Changes of atmospheric environment (fog, haze, precipitation etc.)	Environmental change	Consistent backscattering deviation on entire scene of images, occurred randomly in time	√	×
3	Changes of land surface (rainfall, catchments, soil moisture etc.)	Environmental change	Backscattering deviation on entire scene of images, occurred randomly in time, varied according to land use type	√	×
4	Physical or biological change	Change of vegetation	Backscattering deviation on vegetation area, varied with local farming and climate, seasonal and periodical change, reversible change	×	×
5	LULC change	Manmade change	Irregular and isolated events occurred randomly and widely dispersed throughout the entier scene of images, permanent and irreversible change, few in number	√	√

although the occurrence of such changes was relatively random and their degree was unpredictable, the results they caused in time-series images were usually consistent over the whole scenes of the images. Thus, it can be assumed that environmental changes cause mainly temporal anomalies in time-series images. Another factor that caused changes in time-series images is the physical or biological variations in vegetation. These variations are normally periodic and reversible. They usually occur synchronously throughout the study area and vary gradually with time (as with the paddy field we illustrated in section 1). So these variations did not cause any spatial or temporal anomalies in the time-series images. As a result, changes due to observation system, environment, and variation in vegetation are manifest as either spatial (concurrent) or temporal (synchronous) anomalies in the time-series images. By comparison, LULC changes caused by human activity are irregular and isolated events that change the land surface permanently and irreversibly. They appear to be anomalous in both the spatial and temporal domains in the time-series images. These LULC changes can be detected by applying certain temporal and spatial anomaly detection methods to the time-series images.

Object-Based Image Analysis

In the real world, LULC change usually occurs in object (or parcel) units. We therefore used object-based image analysis in this paper for anomaly detection. Compared with the pixel-based method, object-based image analysis can better describe the boundary of land parcels, using more attributes to describe the features of the objects, such as spectrum, shape, location, texture, etc. In addition, object-based image analysis is more similar to the process of manual interpretation. Hazel (2001) and Onana et al. (2003) found that an object-based method might help improve the accuracy of image analysis. Moreover, Ofer et al. (2005) found that object-based analysis congregates image pixels to the object, making the analysis more efficient. This is especially important when dealing with mass data images such as hyperspectral and SAR images.

To extract objects from images, remote sensing images must be segmented. In this study, the segmentation procedure began with one-pixel objects and then executed an iterative bottom-to-top object-merging. By merging pixels into smaller objects and then merging smaller objects into larger ones, we produced images that were segmented into patches of heterogeneous objects. The heterogeneous objects were then the minimum units for the image analysis that followed.

Change Vector Analysis

Change vector analysis is usually used to trace the process and magnitude of LULC change. Byrne et al. (1980) constructed a change vector on the basis of the principal component analysis of multi-temporal images. Liu et al. (2005) and Li et al. (2005) constructed a change vector for LULC change detection. In our study, we constructed change vectors on the basis of segmented objects. The spectral and texture attributes of each image object were extracted, and the change vector from time to time was calculated by the following formula:

$$X(t-1,t) = \begin{pmatrix} X^t \\ X^{t-1} \end{pmatrix} = \begin{pmatrix} x_1^t, x_2^1, \ldots, x_n^t, \ldots, x_N^t \\ x_1^{t-1}, x_2^{t-1}, \ldots, x_n^{t-1}, \ldots, x_N^{t-1} \end{pmatrix}, \quad (1)$$

where $X^t = (x^t_1, x^t_2, \ldots, x^t_n, \ldots, x^t_N)$ is the eigenvalue vector of an image object at time t, x^t_n is the n-th eigenvalue (of the spectral or texture attributes) of the image object at time t, N is the length of the eigenvalue vector of the object, and $X(t-1,t)$ represents the changes of the eigenvalue vector in magnitude and direction from time $(t-1)$ to t.

Density-Based Anomaly Detection (DBAD)

Density-based anomaly detection was originally proposed by Ramaswamy et al. (2000). They defined a local outlier factor (LOF) to measure the abnormity of object attributes in a dataset. The LOF calculation is simple but time consuming. When a dataset expands, this computing time may become unacceptable. Huang et al. (2005) next proposed a stochastic searching strategy for outlier detection. Their strategy retained some of the advantages of the LOF and reduced the number of neighborhood queries. In this paper, Huang's stochastic searching algorithm was adopted, and its data was extended to the N-dimension eigenvalue space. An N-dimension change vector was constructed and objects were detected on the basis of the distribution of the change vectors. The DBAD algorithm is developed as follows.

First, we define the eigenvalue of the image objects as dataset D. For each image object i ($i \in D$), we have a change vector $X(t-1,t)$ in the eigenvalue space denoted as vector $\bar{p}$ or $\bar{q}$. Here we use the maximum Euclidean distance of change vectors i and change vectors j in t time and $(t-1)$ time, respectively, to evaluate the distance of every two objects i and j. The formula is as follows:

$$dist(\bar{p},\bar{q}) = dist(X_i, X_j) = \quad (2)$$

$$\max\left(\sqrt{\sum_{n=1}^{N} (X^t_{i,n} - X^t_{j,n})^2}, \sqrt{\sum_{n=1}^{N} (X^t_{i,n} - X^{t-1}_{j,n})^2} \right) \quad (i \neq j),$$

where $\bar{p}(\bar{p} = X_i)$ and $\bar{q}(\bar{q} = X_j,\ i \neq j)$ are the change vectors of the i-th and j-th image objects, and X^t_{i-n} is the n-th eigenvalue of the image object i at time t. In formula (2), object i and j will differ greatly from each other no matter whether their Euclidean distance is large at time t or at time $(t-1)$.

For any change vector $\bar{p}$, the impact neighborhood $Neib(\bar{p})$ is defined as

$$Neib(\bar{p}) = \{\bar{q} \in D\},\ where\ \ dist(\bar{p},\bar{q}) \leq Eps,\ and\ \ (\bar{q} \in C), \quad (3)$$

where C is a non-void dataset and Eps is the neighborhood parameter.

If we set $MinVets$ to be the anomaly-detection parameter, then for any change vector $\bar{p}$ and $\bar{q}$ in the eigenvalue space,

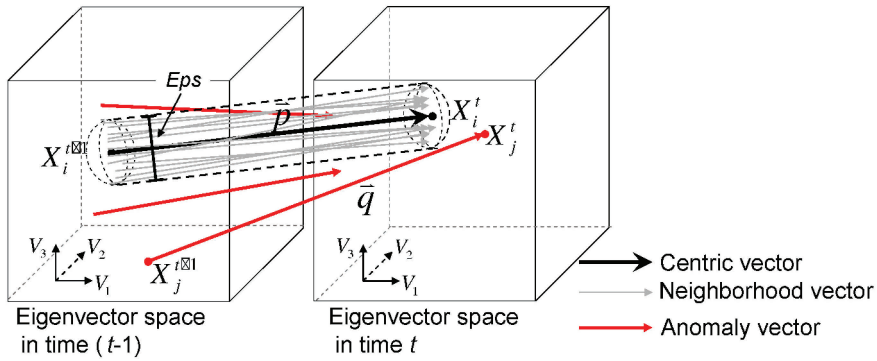

Fig. 1. Schematic diagram of density-based anomaly detection.

if $Neib(\bar{q}) < MinVets$, and $\forall \bar{p} \in D$, if $|Neib(\bar{p})| > MinVets$, then $\bar{q} \notin Neib(\bar{p})$, then $\bar{p}$ is referred to as the centric vector and $\bar{q}$ is referred to as the anomaly vector. $Outlier(\bar{q}) = \{\bar{q} \in D\}$. A schematic diagram of DBAD is shown in Figure 1.

According to the above definition of the density-based anomaly, the anomaly vectors of any two scenes of the time-series images depend not only on the values of the change vectors but also on the density of the change vectors in the eigenvalue space. Isolated or sparsely distributed change vectors are determined to be anomalies in the dataset. Thus, change vectors that are very different from the background change vectors or other synchronous land surface change vectors would be detected as anomaly vectors.

ANOMALY DETECTION AND LULC CHANGE ANALYSIS

Data and Data Preprocessing

The Pearl River Delta of southern China was selected as the study area. Three scenes of repeat-pass RADARSAT imagery were used for change detection. The product used was the RADARSAT Single Look Complex (SLC) with a beam mode of "fine" (F4). RADARSAT repeat-pass imaging indicates the acquisition of imagery under the same conditions (same tracks and same incidence angle); in this case, the incidence angle was 45.08°. The imagery acquisition plan was submitted beforehand to the Canadian Space Agency by the Remote Sensing Ground Station in China so that all the images could be acquired on schedule. Table 2 lists the dates of the data acquisition and the corresponding prior 24 hours' rainfall. Synchronous field surveying was carried out at the same time of the scheduled RADARSAT pass of the research area. Field investigations included the location of the parcels, the LULC types of the parcels, and some description of the parcels, such as the height of the vegetation cover, the coverage of the vegetation, the phenology of the crops, the height of buildings, and so on. A scene of multi-spectral SPOT imagery (spatially enhanced, resolution 2.5 m) acquired at a time close to our research period (Dec 20, 2005) was used together with the field survey. In the production of the field survey, parcel boundaries were drawn on the SPOT image and their attributes recorded. When the field work was finished, the surveyed parcels and their attributes were digitized and stored as a reference layer.

Table 2. Date of Acquired RADARSAT Data and Corresponding Prior 24-Hour Precipitation

Date	24-hour precipitation, mm[a]
January 27, 2006	0.0
March 16, 2006	0.0
May 3, 2006	2.9

[a]Prior to data acquisition.

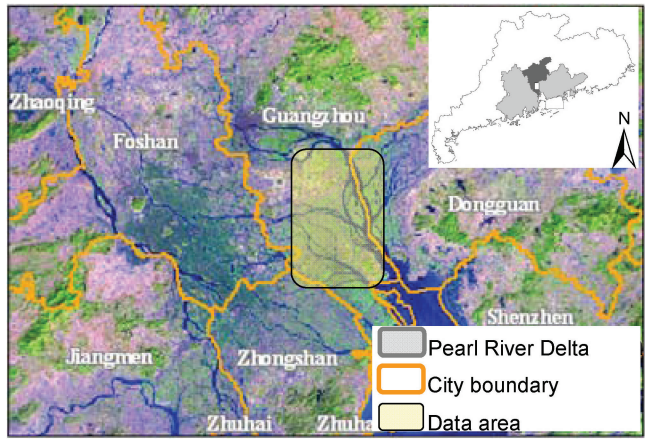

Fig. 2. Location of the study area.

The original pixel size of the RADARSAT SLC data, including the complex I and Q values of the SAR returning wave, was 4.6 × 5.1 m. The software package PCI XPACE Radar Analysis was used to transfer the SLC data to a ground ranged image, which is to say, the backscattering coefficients image. The final pixel size of the georeferenced ground ranged images was 6.25 × 6.25 m. The three scenes of georeferenced RADARSAT images were then precisely rectified to the local topographic map.

The study area was restricted to the overlapping area of the three scenes of the RADARSAT images. Land use and land cover types in this area were mainly those of agricultural land, woodland, and water. In addition, there was also some built-up and residential land in this area. Figure 2 shows the location of the study area.

To reduce the speckle noise in the RADARSAT images, a 5 × 5 gamma filter was applied. The filtered images were then layer-stacked in chronological order. After this, Definiens *e*Cognition software (2004) was used to apply multi-resolution segmentation to the stacked multi-temporal images. Here, we used the same segmentation parameters (Table 3) that Li et al. (2009) used in their multi-temporal RADARSAT images segmentation, which worked on the same area using the same RADARSAT images. The weight 1 means that every single-temporal RADARSAT image gained the same consideration in the segmentation process.

Table 3. Segmentation Parameters of RADARSAT

Parameters	Value
Scale	20
Weight	1
Shape	0.25
Tone	0.75
Compactness	0.9
Smoothness	0.1

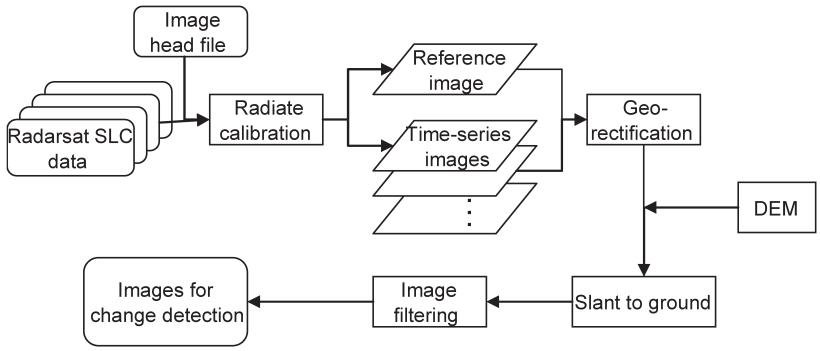

Fig. 3. Data preprocessing of RADARSAT images.

There have been a number of publications concerning segmentation errors in object-based remote sensing. In this paper, no particular evaluation was performed on the accuracy of the segmentation. The reason is that, unlike in object-based classification, in object-based change detection there were no direct multiplicative relationships between image segmentation errors and change detection errors. It is reasonable to assume that only a certain part of the segmentation error would be carried on to the following steps of change detection. Hence, in this paper no accuracy evaluation of the segmentation error was performed. We simply performed an overall evaluation of the change detection in section 3, an evaluation that might be the main concern of our paper.

After segmentation, eigenvalues were extracted for each segmented object. Four eigenvalues (the mean backscatter coefficient of each image object [*Mean*], the minimal backscatter coefficient of each image object [*Min*], the homogeneity of the gray level co-occurrence matrix [*GLCMHomo*], and the dissimilarity of the gray-level co-occurrence matrix [*GLCMdis*]) were then chosen empirically to construct the change vectors. Figure 3 shows the workflow of data preprocessing and Figure 4 shows the segmentation results; Table 4 presents the corresponding change vectors.

Table 4. Example of Two Object-Based Change Vectors

Object ID	Time	Mean	Min	*GLCMHomo*	*GLCMDis*
251	January 27, 2006	–3.20	–7.43	0.12	26.16
	March 16, 2006	–3.42	–5.49	0.12	21.13
	May 3, 2006	–2.42	–5.67	0.13	21.24
252	January 27, 2006	–1.80	–2.73	0.12	22.10
	March 16, 2006	–1.55	–3.67	0.12	25.49
	May 3, 2006	–1.47	–2.69	0.12	25.10

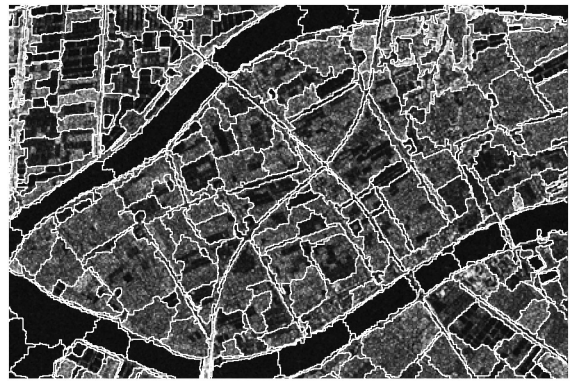

Fig. 4. Result of RADARSAT image segmentation.

Setting of the Change Detection Parameters

In change detection algorithms, the threshold of the differentiation of changed and unchanged pixels in the difference image (the value of image 1 in time t minus the value of image 2 in time $t - 1$) is a very important parameter. As Sheng et al. (2004) observed, the selection of this threshold could decide the overall change detection error. In most cases, these parameters are decided by mainly human experiences. These experiential methods are person dependent and thus not always reliable. There has already been research discussing the way to decide these parameters in a more reasonable way (Chiang et al., 2001; Im et al., 2008). In this paper, abnormal LULC changes were detected by DBAD, which chose the appropriate neighborhood parameter *Eps* and density parameter *MinVets*. It is reasonable to assume that the detected anomalies did not change with the values of the parameters. That is, the number of detected anomalies should be the same for every two image scenes and should equate to the number of real LULC changes in the study area. On the basis of this assumption, we proposed a probing search method to decide the threshold in an objective manner. To achieve this, a subset image was taken from the whole scene of the images, and the DBAD method was applied to the subset. Different *Eps* and *MinVets* values were brought into the DBAD. Then the numbers of detected anomalies were counted for all the possible values of *Eps* and *MinVets*. The results are presented in Figure 5.

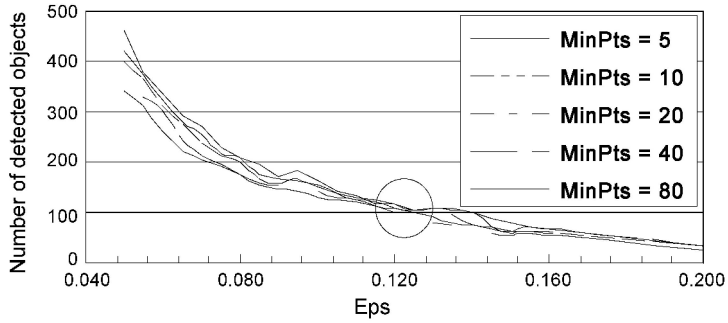

Fig. 5. Curves of detected object numbers and of the parameters *Eps* and *MinVets*.

Figure 5 shows that the number of detected anomalies decreased as *Eps* increased. On the other hand, the number of anomalies increased when *MinVets* increased. When *Eps* was less than 0.1, the detected number increased quickly, whereas *Eps* decreased, and when *Eps* was greater than 1.25, the number of detected anomalies decreased slowly with the increase of *Eps*. When *Eps* was between 0.1 and 0.125, the detected number changed slowly in the range from 110 to 90. The curves corresponding to different *MinPts* intersected at the point where *Eps* is equal to 0.12 and when the detected anomaly objects were approximately 100. At this point, however, the detected anomaly did not vary with the parameter *MinPts*, which ranged from 5 to 80. It was still necessary to choose a median value of *MinPts* to assure that the algorithm was safe and reliable. Hence *MinPts* = 20 and *Eps* = 0.12 were selected as the threshold for the DBAD algorithm.

Results and Verification

Because the study area was located in the estuary area of the Pearl River Delta, ships and tidal shoals inevitably affected the detection results. Therefore, the image objects located in the water bodies were removed from the detection datasets in advance. Only objects located in the land areas (of which there were approximately 19,216 objects) were used in anomaly detection.

Table 2 shows that the three scenes of the images were acquired from late winter to early summer of the following year. According to local phenology, the land surface in this period changed significantly, especially in agricultural and vegetation-covered areas. For example, in January, the paddy fields were fallow, and most paddy fields were covered with bare soil and cropped stems. In March, it was the transplanting season for the paddies. Most of the paddy fields were filled with water. Meanwhile, other agricultural land planting vegetables such as corn and sugarcane were in their growing season. The vegetation coverage of these fields changed with the growth of the leaves and the height of the stems. By May, rice and other crops were still in growth, whereas other vegetables had already matured and were in harvest. Some vegetable fields were bare and some were still covered with in-harvest vegetables. These seasonal changes regularly occurred in our study area and were recorded in the time-series RADARSAT images. It is roughly estimated that more than 50% of the area accounted for over 10% of the backscattering coefficient changes in every two scenes of our study area's

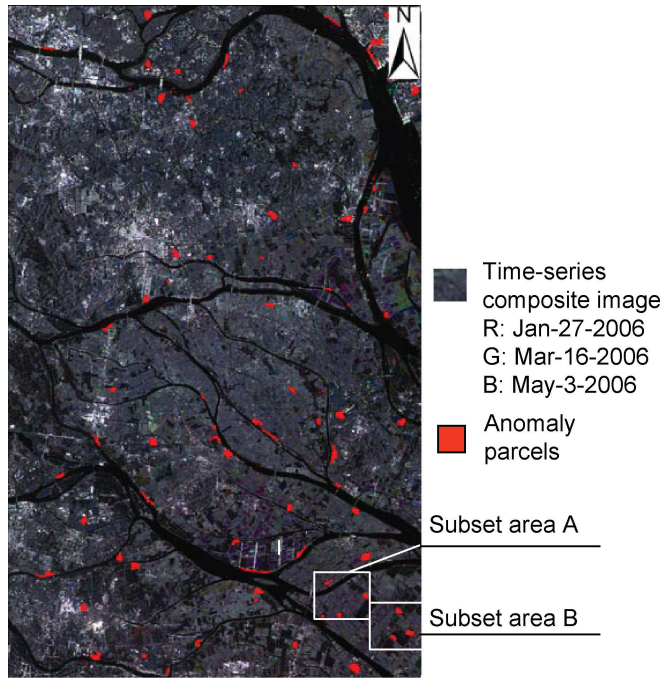

Fig. 6. Results of density-based anomaly detection (DBAD).

images. Such significant backscattering changes could be easily mistaken for LULC change by traditional methods.

As a result, there were a total of 176 anomalous parcels detected by the DBAD algorithm within the study area (Fig. 6). Figure 7 shows the detail of the DBAD results for the subset area A. In Figure 7, four anomalously changed parcels (three large and one small) were detected. The largest two parcels were construction areas (converting from other LULC types to that of a built-up area), and the other two were in the process of conversion from agricultural fields to fishery ponds. As the images show, the backscattering coefficients of the anomalous parcels and their neighboring agricultural parcels all changed remarkably during the observation period (indicated by the colored area in the composite image). The changes in agricultural lands consisted in the rapid growth of vegetation from January to May. However, in the change vector plots, the distribution density of the four detected parcels differed greatly from the densities of the others. Thus, these were detected as abnormally changed objects by the DBAD algorithm.

Figure 8 is another subset area (B) of the DBAD result. In subset area (B), most of the parcels were agricultural land, and there were only four parcels detected as anomalies using the DBAD algorithm. Two of the anomaly parcels changed from agricultural land to fish ponds (the upper left and the upper right ones). The other (the lower left parcel) was a fishpond that was drained, dried by sun, and then refilled with water during the observation period. The last one (the lower right parcel) was a newly built residence. Because the DBAD algorithm detected the density of the change vectors in eigenvalue space, the results were dependent not only on the magnitude and direction

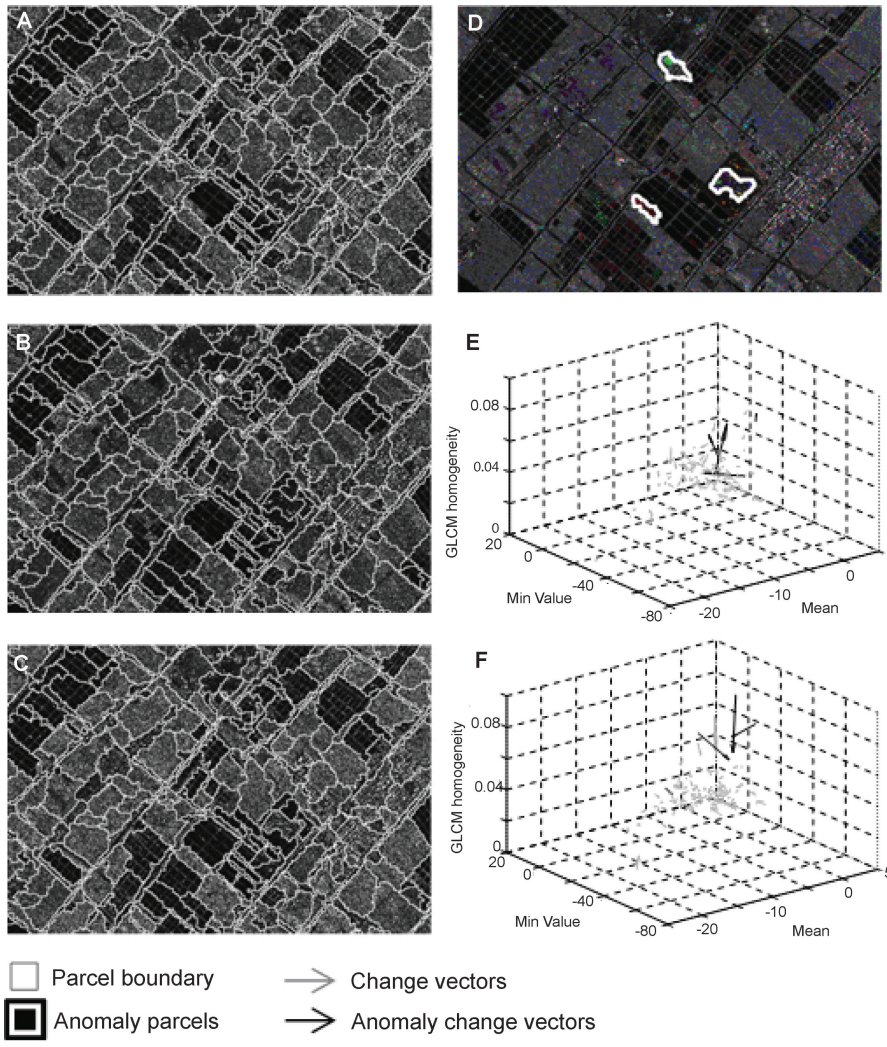

Fig. 7. Results of time-series anomaly change detection. A. SAR image for January 27, 2006. B. SAR image for March 16, 2006. C. SAR image for May 3, 2006. D. Detected anomalous parcels and time-series composite image: red = January 27, 2006; green = March 16, 2006; blue = May 3, 2006. E. Change vectors from January 27, 2006 to March 16, 2006. F. change vectors from March 16, 2006 to May 3, 2006.

of the change vectors but also on the density of the change vectors in the eigenvalue space. As a result, the remarkable image changes caused by vegetation growth, which were common in the study area (as well as the colored areas in the composite image), were excluded from the real LULC change measurements because of the high densities of the change vectors. Only four distinctive change vectors were detected as anomalies, corresponding exactly with LULC changes in the real world. Such differentiation was almost impossible using traditional image comparison methods.

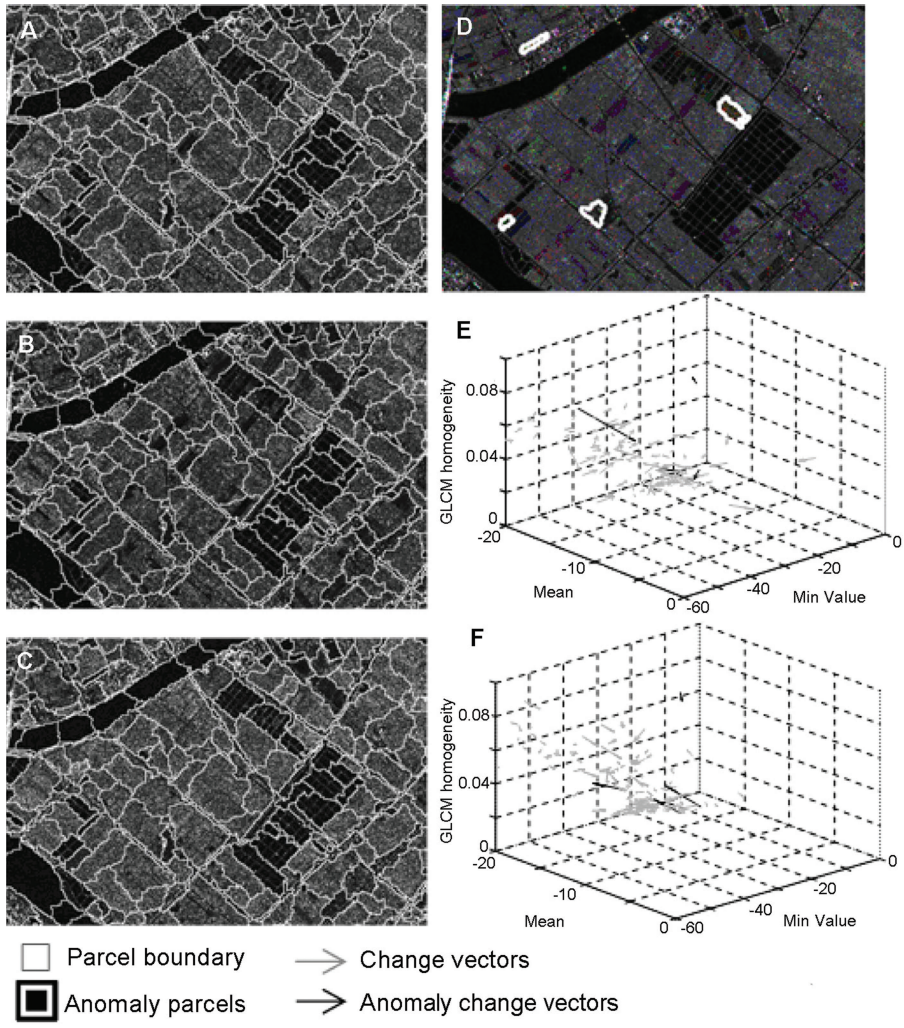

Fig. 8. Results of time-series anomaly detection. A. SAR image for January 27, 2006. B. SAR image for March 16, 2006. C. SAR image for May 3, 2006. D. Detected anomalous parcels and time-series composite image: red: January 27, 2006; green: March 16, 2006; blue: May 3, 2006. E. Change vectors from January 27, 2006 to March 16, 2006. F. Change vector from March 16, 2006 to May 3, 2006.

In sum, the above examples show that although images varied noticeably in the RADARSAT time series, the distribution densities of the LULC changed parcels in their change vector space were apparently different from those of the seasonal vegetation changes or environmental changes. Thus, the DBAD method could be used for LULC change detection in time-series images that concern not only the value of the change vectors but also the distribution of the change vectors. The detection result shows obvious differences from the regular change detection result.

Finally, the results were validated using field survey data. Just as most publications have stated (Weidner, 2008; Zhan et al., 2005), object-based image analysis

concerns not only pixel-by-pixel classification (or change detection) error, but also object-by-object geometric error. So, in this paper, change detection errors were evaluated both in terms of objects (parcels) and in terms of pixels. To evaluate the result in pixels, all the detected parcels and the field-surveyed parcels were rasterized to 6.25 × 6.25 m resolution. To evaluate the result in parcels, the segmented image parcels were compared to the field-collected parcels in their spatial and LULC attributes. Here we prescribed that detected parcels that were completely within the referenced parcel or that shared more than 80% of their area with the referenced parcels were regarded as correct in location. Then, the change attributes of the detected parcels were evaluated relative to the reference data. To evaluate the detection capability of the DBAD algorithm for different LULC change classes, the parcel-based detection accuracies were calculated in terms of each change class.

Table 5 lists all the actual LUCC change detected by field surveying and the detection errors of the parcel-based DBAD. In Table 5, the highest detection accuracy was achieved in newly built-up land parcels or in land parcels under construction (with a failed alarm rate of less than 13.3%). A relatively low detection error was achieved in woodlands (false alarm rate error less than 8.3%), which owes to the stability of the woodlands in the observation periods. The failed alarms in agricultural land and fish ponds were between 12.5 and 25.0%. The error in fish ponds was mainly caused by changes of the shoals and riverbanks. A relatively large detection error was obtained in built-up areas and in agricultural land, including construction areas, rural residential areas, and some mixed-use areas (with false alarm rates between 16.7 and 20.0%). The error was mainly due to the internal complexity and multiformity of the built-up areas and the agricultural land. In these areas, the backscattering coefficient varied with the parcels and with time. Hence, some of these parcels might have been mistaken as anomalies by the DBAD algorithm. Incorrect segmentation also introduced some error to DBAD. This always occurred for the objects that were located at the boundary of the parcels or within some mis-georectified area.

In the end, a pixel-based change vector was constructed and a pixel-based DBAD algorithm was tested in comparison with the object-based DBAD algorithm. In pixel-based DBAD, image texture homogeneity and dissimilarity were calculated through PCI Radar Analysis. The change vectors were constructed using the backscattering coefficient, homogeneity, and dissimilarity. The accuracy assessment listed in Table 6 shows that, in comparison to pixel-based DBAD (overall accuracy 76.9%), object-based DBAD produced better overall accuracy (84.4%). The overall kappa for changed and unchanged classes also revealed that the object-based DBAD (0.69) produced more satisfactory accuracy than the pixel-based method (0.53). That is, benefitting from the homogeneously merged pixels set, the object-based DBAD algorithm achieved a higher accuracy than did the pixel-based method.

CONCLUSION

Based on the above experiments, the DBAD algorithm was able to detect anomalous changes in time-series images that suffered significantly from changeable environments and variable observation systems. By applying a stochastic searching strategy to the algorithm, the DBAD algorithm effectively detected the anomalously changed objects by removing regularly and consistently changed objects from the datasets.

Table 5. Validation of DBAD Results

Changed land parcels				Unchanged land parcels			
Types	Sampled parcels	Anomaly parcels	Failed alarm, %	Types	Sampled parcels	Anomaly parcels	False alarm, %
Bare land→built-up area	15	13	13.33	Built-up area	12	2	16.67
Bare land →agricultural land	12	10	16.67	Bare land	18	2	11.11
Fishpond→agricultural land	9	7	22.22	Agricultural land	25	5	20.00
Agricultural land→fish pond	8	7	12.50	Woodland	12	1	8.33
Agricultural land→built-up area	9	8	11.11				
Agricultural land→bare land	8	6	25.00				

Table 6. Comparison of object-based DBAD and pixel-based DBAD

	Object-based	Pixel-based
Failed alarm (%)	16.4	22.9
False alarm (%)	14.9	23.2
Overall accuracy (%)	84.4	76.9
Overall kappa	0.69	0.53

The experiment used a set of SAR time-series images over the cloudy and rainy area of southern China and confirmed that the DBAD algorithm was capable of detecting LULC changes in the short term. The results showed that the algorithm performed outstandingly in detecting areas of new construction or of construction in-progress, including areas changing from bare to built-up land or from agricultural to built-up land. By calculating the distribution density of the change vectors in the eigenvalue space, the LULC change parcels could be easily differentiated from the other land parcels. Although the land parcels in our study area were fragmented and the vegetation types diverse, making the LULC change detection relatively difficult, it was still possible to detect suspicious changes by way of the DBAD algorithm.

In this study, the DBAD algorithm only detected change parcels from short-term time-series images. It did not provide the detailed "from-to" information for particular parcels that was also significant in LULC change. In order to acquire accurate "from-to" information from DBAD results, quite a lot work remains to be done. Thus we propose that the results of DBAD be used together with other methods for further validation or classification.

Compared with traditional image comparison methods, DBAD is an unsupervised method that does not require prior knowledge or high-quality training data. Because DBAD takes both global and local changes into consideration, it can remove changed image-objects caused by the observation system or the environment and detect the objects caused by "real" LULC change. This makes DBAD a powerful change detection tool that could work in a variety of environmental situations.

As an all-weather operable observing system, SAR imagery was an ideal source of data for short-term LULC change detection. Although SAR time-series images collected data in short time intervals and had recorded all the observable seasonal changes and changes caused by the observation system or the environment, the anomaly detection method proposed in this paper could effectively correct these data by extracting the real LULC change from other "false" changes. This helps to improve the accuracy of short-term LULC change detection.

In addition, we used just four relatively simple metrics in this study to construct our change vectors. These variables were chosen by expert experience. The results showed that these four variables worked well in our algorithm. Although there is no reason to believe that more variables or another combination of variables would increase the detection accuracy, we suggest that further research be done on the construction or optimization of the change vectors.

ACKNOWLEDGMENTS

This paper was supported by the Hong Kong Research Grants Council (RGC) (HKU 7301/04H) and partially supported by National Natural Science Foundation of China (40071060).

REFERENCES

Barnett, V. and T. Lewis, 1994, *Outliers in Statistical Data*, New York, NY: John Wiley, 584 p.

Byrne, G. F., Crapper, P. F., and K. K. Mayo, 1980, "Monitoring Land-Cover Change by Principal Component Analysis of Multi-temporal Landsat Data," *Remote Sensing of Environment*, 10:175–184.

Chen, M., Yi, Y. H., and D. R. Li, 2006, "Application of Projection Pursuit Based on Dynamical Evolutionary Algorithm to Anomaly Target Detection in Hyperspectral Images," *Geomatics and Information Science of Wuhan University*, 31(1):55–58.

Chen, T. and Z. L., Li, 2006, "A Multiscale Approach for Spatio-temporal Outlier Detection," *Transactions in GIS*, 10(2):253–263.

Chen, X. X., Lee, V. and D. Deering, 2005, "A Simple and Effective Radiometric Correction Method to Improve Landscape Change Detection across Sensors and across Time," *Remote Sensing of Environment*, 98:63–79.

Chiang, S. S., Chang, C. I., and I. W. Ginsberg, 2001, "Unsupervised Target Detection in Hyperspectral Images Using Projection Pursuit," *IEEE Transactions on Geoscience and Remote Sensing*, 39:1382–1391.

Definiens, 2004, *E-Cognition Professional 4.0 User Guide*, Munich, Germany: Definiens Imaging, 475 p.

Gauthier, R. P., Maloley, M., and K. B. Fung, 2001, "Land-Cover Anomaly Detection along Pipeline Rights-of-Way," *Photogrammetric Engineering And Remote Sensing*, 67(12):1377–1389.

Hawkins, D., 1980, *Identification of Outliers*, London, UK: Chapman and Hall, 188 p.

Hazel, G. G., 2001, "Object-Level Change Detection in Spectral Imagery, *IEEE Transactions on Geoscience and Remote Sensing*, 3:553–561.

Huang, T. Q., Qin, X. L., Chen, C. C., and Q. M. Wang, 2005, "Density-Based Spatial Outliers Detecting," *Proceedings Lecture Notes in Computer Science*, 3514:979–986.

Im, J. H., Jensen, J. R., and M. E. Hodgson, 2008, "Optimizing the Binary Discriminant Function in Change Detection Applications," *Remote Sensing of Environment,* 112(6):2761–2776.

Kou, Y., Lu, C. T., and D. Chen, 2006, "Spatial Weighted Outlier Detection," in *The 2006 SIAM Conference on Data Mining*, April 2006, Bethesda, MD, 613–617.

Li, D. R., 2003, "Change Detection from Remote Sensing Images," *Geomatics and Information Science of Wuhan University*, 28:7–12.

Li, X., Yeh, A. G. O., Qian, J. P. et al., 2009, "A Matching Algorithm for Detecting Land Use Changes Using Case-Based Reasoning," *Photogrammetric Engineering & Remote Sensing,* 75(11):1319–1332.

Li, Y. C., Chen, J., Gong, P., and Yue, T. X., 2005, "Study on Land Cover Change Detection Method Based on NDVI Time Series Datasets: Change Detection Indexes Design," *Journal of Basic Science and Engineering,* 13(3):261–275.

Liu, D. L. and J. Q. Zhang, 2006, "Approach of Texture-Based Anomaly Detection for Remote Sensing Imagery," *Journal of Infrared and Millimeter Waves*, 25(3):236–240.

Liu, J., Gong, P., P. J. Shi et al., 2005, "Study on Change Detection Automatically Based on Similarity Calibration*," Journal of Remote Sensing*, 9(5):537–543.

Lu, W., Yu, X. C., Liu, J., and G. P. Yang, 2006, "A Small Targets Detection Approach Based on Anomaly Distributing in Hyperspectral Imagery*," Acta Geodaetica et Cartographica Sinica*, 35(1):40–45.

Nagler, T. and H. Rott, 2000, "Retrieval of Wet Snow by Means of Multitemporal SAR Data," *IEEE Transactions on Geoscience And Remote Sensing*, 38(2):754–765.

Ofer, M., Arie, P., and A. Amir, 2005, "Objects-Based Change Eetection in a Pair of Gray-Level Images," *Pattern Recognition*, 38:1976–1992.

Onana, V. P., Trouve, E., Mauris, G., Rudant, J. P., and Frison, P. L., 2003, "Change Detection in Urban Context with Multitemporal ERS-SAR Images by Using Data Fusion Approach," in *IGARSS 2003: IEEE International Geoscience and Remote Sensing Symposium*, I–IV:3650–3652.

Praks, J., Alasalmi, H., and M. Hallikainen, 2001, "Polarimetric Properties of Boreal Forest in L- and C-band SAR Images," in *IEEE International Symposium on Geoscience and Remote Sensing (IGARSS)*, 3050–3052.

Qian, J. P., Li, X.,Yeh, A. G. O., Ai, B., Liu, K., and X. Y. Chen, 2007, "Radarsat Time Series Analysis and Short-Time Change Detection of Regional Land-Use/Land-Cover," *Journal of Remote Sensing*, 11(6):931–940.

Quegan, S., Le Toan, T., J. J. Yu et al., 2000, "Multitemporal ERS SAR Analysis Applied to Forest Mapping," in *IEEE Transactions On Geoscience And Remote Sensing*.

Ramaswamy, S., Rastogi, R., and K. Shim, 2000, "Efficient Algorithms for Mining Outliers from Large Data Sets," in *SIGMOD Conference 2000*, *New York*, 979–986.

Sheng, H., Liao, M. S., and L. Zhang, 2004, "Determination of Threshold in Change Detection Based on Canonical Correlation Analysis," *Journal of Remote Sensing*, 8(5):451–457.

Song, C. H., Woodcock, C. E., Seto, K. C., Lenney, M. P., and S. A. Macomber, 2001, "Classification and Change Detection using Landsat™ Data: When and How to Correct Atmospheric Effects?," *Remote Sensing of Environment*, (75):230–244.

Stabel, E. and P. Fischer, 2001, "Satellite Radar Interferometric Products for the Urban Application Domain," *Advances in Environmental Research*, 5(4):425–433.

Weidner, U., 2008, "Contribution to the Assessment of Segmentation Quality for Remote Sensing Applications," in *International Archives of Photogrammetry and Remote Sensing,* Vol. XXXVII, Part B7, Beijing, 479–484.

Zhan, Q., Molenaar, M., Tempfli, K., and W. Shi, 2005, "Quality Assessment for Geospatial Objects Derived from Remotely Sensed Data," *International Journal of Remote Sensing*, 26(14):2953–2974.